

OPTIMAL DESIGN AND MULTIBODY ANALYSIS OF RZEPPA PILOT-LEVER JOINT

Ettore Pennestrì*, P.P. Valentini*, R. Stefanelli*

*Dipartimento di Ingegneria Meccanica
Università di Roma Tor Vergata, Via del Politecnico 1, 00133 Roma, Italy
e-mail: pennestri@mec.uniroma2.it, web page: <http://ingegneriameccanica.org>

Keywords: Mechanical joints, Rzeppa joint, homokinetic joint.

Abstract. *Rzeppa pilot-lever joint represents a classical solution to the problem of transmitting torque between angularly misaligned shafts. Homokineticity is one of the most important requirement in industrial applications. The Myard's theorem gives the geometrical conditions which ensure the satisfaction of such requirement. In this paper two different original proofs of this theorem are offered.*

An algorithm for the optimal kinematic synthesis of the pilot-lever mechanism is then proposed. The pilot lever mechanism is designed to minimize the maximum angle between the transmission and the homokinetic plane.

Finally, a multibody dynamic analysis of the Rzeppa pilot-lever joint is made by means of a commercial software. The modeling of contact conditions between the balls the the guides is in particular discussed. Finally, the contact forces between spheres and guides for different angles between input and output shafts are computed.

1 Nomenclature

- a_1 and a_2 : Axes of the shafts coupled with the joint;
- h and k , link length ratios;
- α : Angle between the axes a_1 and a_2 ;
- α_d : Angle between transmission and homokinetic planes;
- ω_1 and ω_2 : Angular speeds of the coupled shafts;
- θ : Angle between the normal to the transmission plane and the a_2 axis;
- θ_1 and θ_2 : Related angles of rotations of the coupled shafts;

2 Description of the Rzeppa joint

The Rzeppa joint usage began in 1936 in front-wheel drive passenger cars produced in the USA. Its distinctive capability is to transmit torque between inclined shafts at almost constant velocity. However, it has been also used in applications such as aircraft, marine, industrial stationary drive systems.

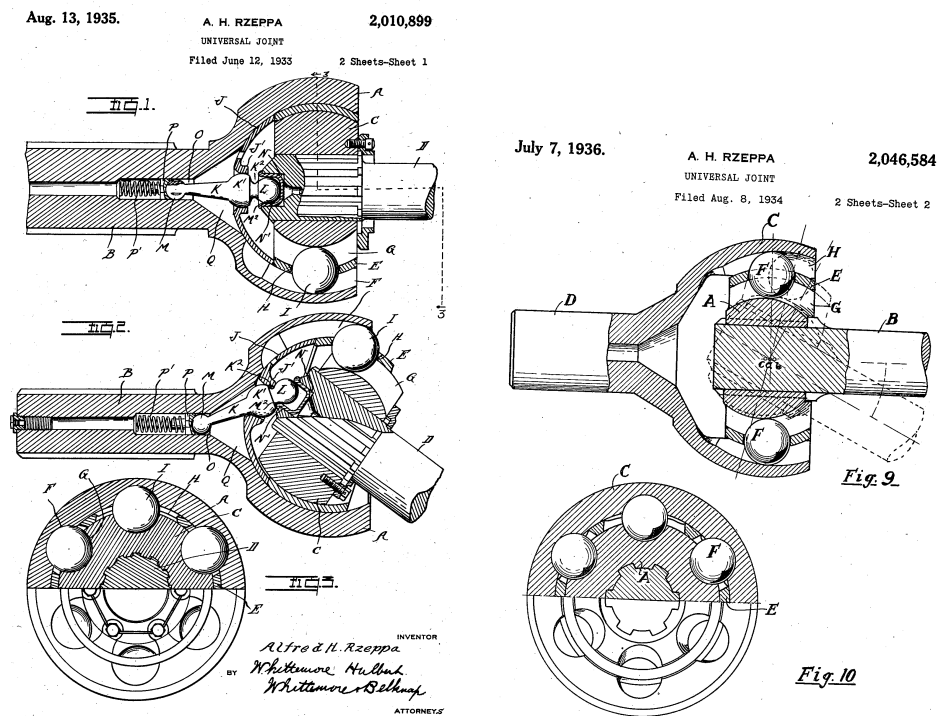


Figure 1: Pilot lever Rzeppa Joint (left) and Rzeppa Joint (right)

In Figure 1 two different types of Rzeppa patented joints are shown [1, 2]. Classical monographies mainly dedicated to the kinematics and design of the Rzeppa joint are authored by Wagner [5], Schmelz *et al.* [4], Duditza *et al.* [6], Bongiovanni and Roccati [3]

In this paper, the so called Rzeppa Pilot-Lever will be studied. The joint connects two shafts B and D with intersection axes. In the following the main components of the joint are briefly described.

- At the extremity of shaft B there is an outer hollow spherical member named A in the drawing. This spherical member has a series of meridian groove ball races whose circular axes are centered on the rectilinear axis of shaft B .
- At the extremity of shaft D there is an inner spherical member named C . This spherical member has also a series of meridian groove ball races whose circular axes are centered on the rectilinear axis of shaft D .
- Between the inner and outer spherical members there is a spherical cage named E with circumferential slots receiving the spheres which engage the spherical slots of A and C .
- The angular position of E is adjusted by a pilot lever mechanism whose purpose is to keep the plane containing the centers of the spheres (transmission plane) as close as possible to the plane midway between the plane of rotation of shafts B and D (homokinetic plane).

As will be demonstrated in this paper, the pilot lever mechanism cannot ensure, for all relative angular positions of the input-output shafts, that all the centers of the spheres are contained in the homokinetic plane. However, it will be possible to execute the kinematic synthesis of the pilot lever mechanism in order to fulfill as close as possible the above geometric condition.

In the pilot lever mechanism there is a force closure kinematic pair. In fact, the axial spring, embedded in the axis B , maintains the contact between kinematic elements.

3 The Myard's theorem

The Myard's theorem states the condition required to obtain constant transmission ratio in a mechanical joint. With reference to the geometry of Figure 2, let the coupling transmit the motion between the shafts with axes a_1 and a_2 . The axes of revolute pairs r_1 and r_2 always intersect in K .

Since

$$C_1K = C_1C_2 + C_2K \quad (1)$$

and $C_1K = h_1 \tan \theta_1$, $C_1C_2 = d$ and $C_2K = h_2 \tan \theta_2$, then the relation between the rotations θ_1 and θ_2 of the axes is

$$\tan \theta_2 = \frac{d}{h_2} + \frac{h_1}{h_2} \tan \theta_1 . \quad (2)$$

By time differentiation of (2) one obtains the transmission ratio

$$\tau = \frac{\omega_2}{\omega_1} = \frac{h_1}{h_2 \cos^2 \theta_1} \frac{1}{\left[1 + \left(\frac{d + h_1 \tan \theta_1}{h_2} \right)^2 \right]} . \quad (3)$$

The homokinetic condition, (*i.e.* $\tau = 1$), is always satisfied when $d = 0$ and $h_1 = h_2$. In other terms, it is required that:

- the axes a_1 and a_2 are incident (*i.e.* $d = 0$);
- point M is contained in the bisector plane (also named *homokinetic plane*) of such axes.

By comparing the geometry of Figure 3 with the one of Figure 2 one can conclude that

$$h_1 = A_1 C_1 \cdot \sin \left(\frac{\pi - \alpha}{2} - \alpha_d \right) = A_1 C_1 \cdot \cos \left(\alpha_d + \frac{\alpha}{2} \right), \quad (5)$$

$$h_2 = A_1 C_1 \cdot \sin \left(\frac{\pi - \alpha}{2} + \alpha_d \right) = A_1 C_1 \cdot \cos \left(\alpha_d - \frac{\alpha}{2} \right). \quad (6)$$

Thus, the ratio $\frac{h_1}{h_2}$, which appears in (3) can be expressed as a function of α_d and α , is expressed by

$$\frac{h_1}{h_2} = \frac{\cos \left(\alpha_d + \frac{\alpha}{2} \right)}{\cos \left(\alpha_d - \frac{\alpha}{2} \right)}. \quad (7)$$

Substituting $d = 0$ and (7) into (3), one obtains the transmission ratio, fully consistent with the one obtained by Fischer and Remington [7], but through a different procedure.

3.1 An alternative proof

A more concise proof of the Myard's theorem can be obtained by considering the spatial extension of the Aronhold-Kennedy theorem.

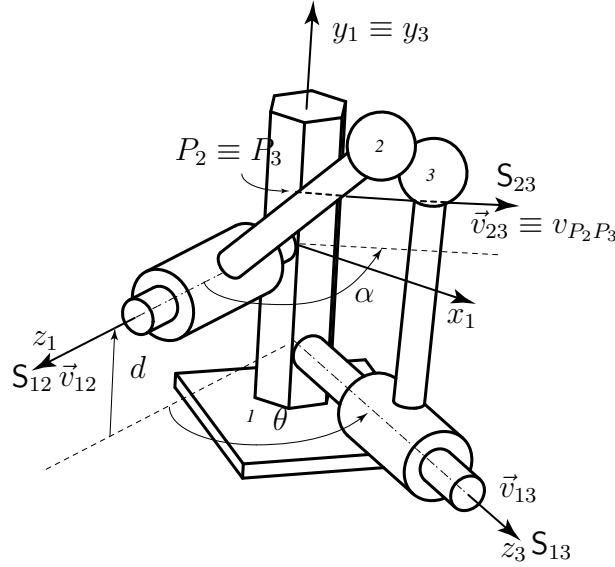


Figure 4: Generalization of Aronhold-Kennedy theorem: Nomenclature

With reference to the geometry of Figure 4, let θ and d be the angle and minimum distance between input and output shaft axes, respectively.

Imposing the homokineticity condition $\omega_1 = \omega_2 = \omega$, one can demonstrate that the relative motion instantaneous screw axis S_{23} is in the intersection of the following planes [9]

$$x_1 = \frac{\omega \sin \theta}{\omega - \omega \cos \theta} z_1 = \frac{z_1}{\tan \frac{\theta}{2}}, \quad (8)$$

$$y_1 = d \frac{\cos \theta - 1}{2(1 + \cos \theta)}. \quad (9)$$

The first equation clearly demonstrates that the homokinetic plane bisects the angle θ .

4 Kinematic analysis and optimal design of the pilot-lever linkage

4.1 Kinematic analysis

The pilot-lever mechanism is composed of three spherical and two slider joints.

In the plane of the two axes a_1 and a_2 , the pilot-lever linkage can be interpreted as a planar six-bar function generator linkage [8] (see Figure 5a). In particular, assumed α as input variable, the output variable is θ . The structural error of this linkage is α_d as defined from equation (4).

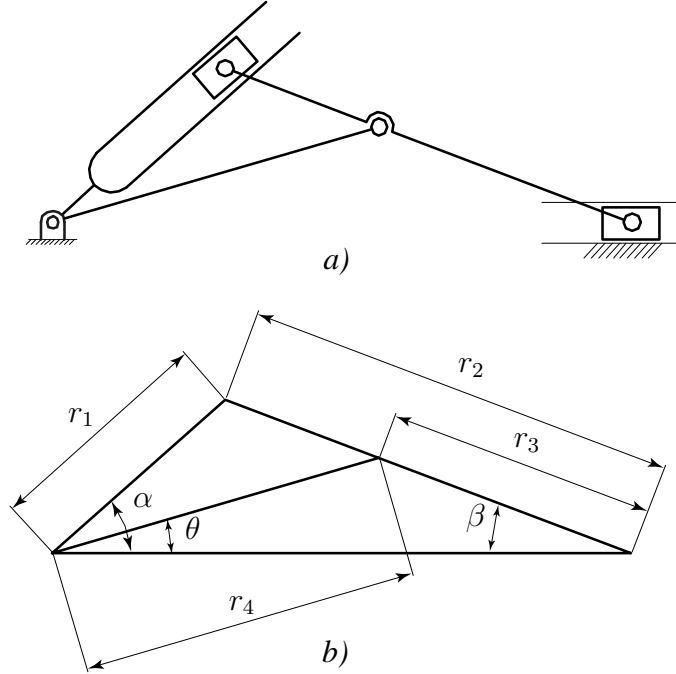


Figure 5: Pilot-lever linkage: Main dimensions

From the geometry of Figure 5b) the following relationships can be established:

$$\frac{\sin \beta}{r_4} = \frac{\sin \theta}{r_3}, \quad (10)$$

$$\frac{\sin(\alpha + \beta)}{r_4} = \frac{\sin(\alpha - \theta)}{r_{23}}, \quad (11)$$

where $r_{23} = r_2 - r_3$. Substituting the first relationship into the second and considering that

$$\cos \beta = \sqrt{1 - \left(\frac{r_4}{r_3} \sin \theta\right)^2}, \quad (12)$$

after some manipulations, one obtains

$$2q \sin 2\theta - p \cos 2\theta + 2r + p = 0, \quad (13)$$

where

$$p = \tan^2 \alpha \left[\left(\frac{r_4}{r_{23}} \right)^2 - \left(\frac{r_4}{r_3} \right)^2 \right] - \left(\frac{r_4}{r_{23}} + \frac{r_4}{r_3} \right)^2, \quad (14)$$

$$q = \tan \alpha \left[\left(\frac{r_4}{r_{23}} \right)^2 + \frac{r_4^2}{r_3 r_{23}} \right], \quad (15)$$

$$r = \tan^2 \alpha \left[1 - \left(\frac{r_4}{r_{26}} \right)^2 \right]. \quad (16)$$

The solution of (13) is expressed by

$$\tan \theta = \frac{-q + \sqrt{q^2 + r(p+r)}}{(p+r)} \quad (17)$$

4.2 Kinematic synthesis

The kinematic synthesis problem can be stated as follows

Compute the link length ratios

$$h = \frac{r_4}{r_2}, \quad (18)$$

$$k = \frac{r_3}{r_2}, \quad (19)$$

such that the structural error α_d is minimized within the feasible range of α .

In order to readily use (17), the following equalities are useful:

$$\frac{r_4}{r_3} = \frac{h}{k}, \quad \frac{r_4}{r_{23}} = \frac{1-k}{h}. \quad (20)$$

Table 1: Optimal values of h and k for $\alpha_{\min} = 0^\circ$, $\alpha_{\max} = 45^\circ$ and maximum values of the structural error.

h^*	k^*	$\alpha_{d\max}$
0.7500	0.7085	2.14°
0.6875	0.7265	1.99°
0.6250	0.7453	1.85°
0.5625	0.7649	1.72°
0.5000	0.7856	1.60°

The feasible ranges of h and k are, respectively,

$$0.50 \leq h \leq 0.75, \quad (21)$$

$$0.65 \leq k \leq 0.80, \quad (22)$$

whereas $0 \leq \alpha \leq \alpha_{\max}$.

Data: $h_{\min}, h_{\max}, k_{\min}, k_{\max}, \alpha_{\min}, \alpha_{\max}$

Result: Optimal values h^* and k^*

for $h = h_{\min}, h_{\max}$ **do**

for $k = k_{\min}, k_{\max}$ **do**

for $\alpha = \alpha_{\min}, \alpha_{\max}$ **do**

 Compute θ by means (17);

 Compute $\alpha_d = |2\theta - \alpha|$;

end

end

 Obtain the values of h^* and k^* which minimize the maximum value of $|\alpha_d|$ within the prescribed range of α ;

end

Algorithm 1: Kinematic synthesis of the pilot-lever linkage

By means of the synthesis procedure outlined in the Algorithm 1, different optimal values of h and k can be obtained (see Table 1). The Figure 4.2 shows the plot of α_d .vs. α for $h = 0.7500$ $k = 0.7085$.

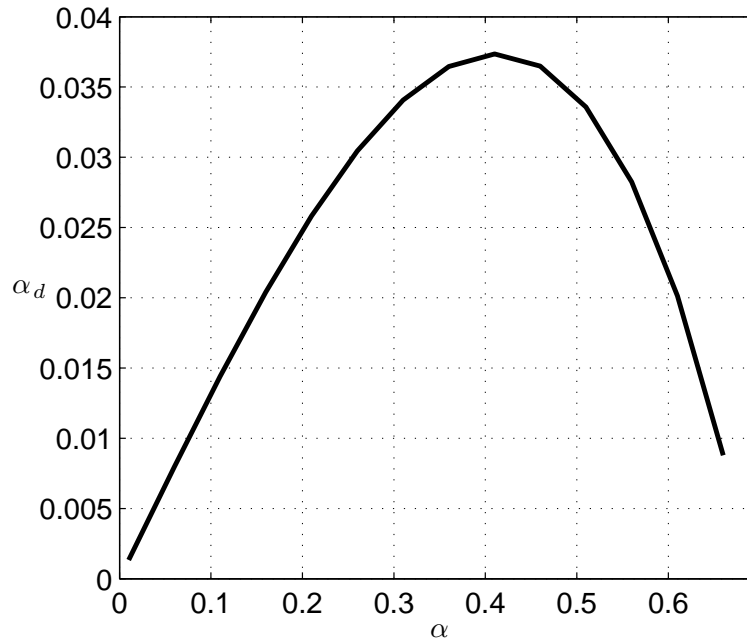


Figure 6: Value of α_d for $h = 0.7500$ $k = 0.7085$.

5 Multibody analysis of the Rzeppa joint by means of commercial software

In order to simulate the dynamics of the R-Zeppa ball joint, a three-dimensional multibody model has been built using the Cosmos/Motion which is a SolidWorks plug-in. The model is made of 11 bodies: the frame, two shafts, the cage, the pilot lever and six balls (Figure 7, on the left). Both shafts are constrained to the frame with revolute joints. Moreover, the centres of the two spherical ends of pilot lever are set coincident to the two shaft axes, while the centre of the third sphere in the middle of the lever is set to be coincident to its housing in the cage. All the centres of the balls are constrained to be coincident to their housings in the cage. The contact conditions between the balls and the meridian grooves of the shafts have

been replaced with only two point-to-curve constraints. It means that the centre of one ball is set to be coincident to two curves (two meridians) on the two shaft (Figure 7, on the right). Only one ball has been constrained in order to avoid joint redundancy. The other balls are included in the models only for taking into account the right inertia properties of the assembly. A stabilizing stiff spring/damper element has been also added between one end of the pilot lever and one end of the outer shaft. An input constant velocity has been applied to the revolute joint degree-of-freedom at the inner shaft and a resisting torque has been applied to the outer shaft. The main purposes of the model are to verify the kinematic irregularities and to assess the forces entity between the balls and the grooves. Since the assessment of these forces is made neglecting the surface elasticity, only a global estimation of the overall dynamics entities is obtained. Thanks to the parametric approach used to build the model, several scenarios have

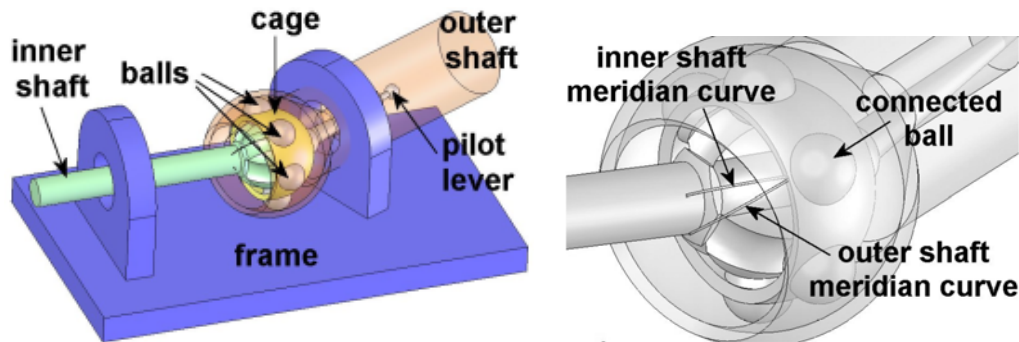


Figure 7: The R-Zepa multibody model (on the left) and a detail of the point-to-curve constraints (on the right)

been simulated, changing the relative configuration between the two shafts. Once assembled the model confirmed the magnitude of kinematic errors on the attitude of the transmission plane with respect to the homokinetic plane, due to the synthesized geometry of the pilot lever. For the same reason the irregularities on the output shaft velocity are the same of the kinematic analysis presented in the previous section of the paper. The additional information that can be evinced from the multibody dynamics simulation is about the estimation of the contact forces between the balls and the grooves which have to be exerted in order to transmit the torque.

The computation of these forces is not directly obtained from the software, but requires further analysis. The authors experienced that even imposing a constraint on the motion of only one ball leads to inaccurate computation of dynamic reactions. Four different forces act on the constrained ball:

- two forces due to the contact with the meridian curves;
- one due to the contact with the cage (which constrains the ball to lay in the transmission plane);
- one due to inertial properties.

During the rotation of the shafts, when the planes of the two meridian curves are coincident, due to symmetry, the solution of the Lagrange multipliers leads to indeterminacy. This behaviour can be avoided by computing the reaction forces exerted between the ball and the curves using geometrical observations. The forces on the ball can be evaluated imposing the equilibrium on the ball, starting from the knowledge of its acceleration state. Thus, the computational steps for computing these reaction forces are the following:

1. Let us start from the expression of the contact force between the ball and the output shaft groove as a function of output resisting torque:

$$\vec{T}_{out} = \vec{F}_{out} \times \vec{r}_{out}(\theta_{out}) \quad (23)$$

where

- \vec{T}_{out} is the resisting torque vector acting on the output shaft;
- \vec{F}_{out} is the contact force between the ball and the meridian curve on the output shaft;
- $\vec{r}_{out}(\theta_{out})$ is the distance vector between the centre of the ball and the output shaft. Please observe that it depends on the angular position of the input.

2. Imposing the force equilibrium of a ball one obtains

$$m_{ball}\vec{a}_{ball} = \vec{F}_{in} + \vec{F}_{out} + \vec{F}_{cage} \quad (24)$$

where

- m_{ball} is the mass of the ball;
- \vec{F}_{in} is the contact force between the ball and the meridian curve on the input shaft (its direction is perpendicular to the tangent vector of such curve);
- \vec{F}_{cage} is the contact force between the ball and the meridian curve on the input shaft (its direction is perpendicular to the transmission plane).

Since the (24) can be decomposed into three scalar equations and it contains 3 unknown variables, namely the two \vec{F}_{in} components and the magnitude of \vec{F}_{cage} , it can be solved by substituting (23).

The computation of the reaction forces \vec{F}_{in} and \vec{F}_{out} has been performed for 3 of optimal configurations taken from Figure 4.2 and summarized in Table 2

Table 2: Main data of test cases analyzed

Test case No	α (deg)	α_d (deg)
1	15°	1.75°
2	20°	2.07°
3	25°	2.10°

The remaining model properties are $\omega_{in} = 1$ rad/s, $T_{out} = 1$ Nm, $m_{ball} = 5$ g. With reference to the Figure 8, it can be notice that the contact forces present a periodic trend with the same period of the transmission irregularities (even when the transmission plane is coincident to the homokinetic one). This means that vibrations and contact fatigue phenomena occur. The frequency of excitation is twice that of the input shaft rotation. The amplitude of contact forces depends on two parameter: the irregularities due to the difference between the transmission plane and the homokinetic one, and the angular misalignment between shafts. With the same

kinematic error α_d , the irregularities are wider if the planes are more misaligned. When $\alpha_d \rightarrow 0$ the contact forces between ball and input shaft groove and between ball and output shaft groove are the same. When α_d increases the two forces are slightly different and their difference produce an increase of cage reaction force. This hints that kinematic errors cause two structural problems: a loading of elements with frequency double of the angular speed and an increase of the internal forces which do not contribute to torque transmission.

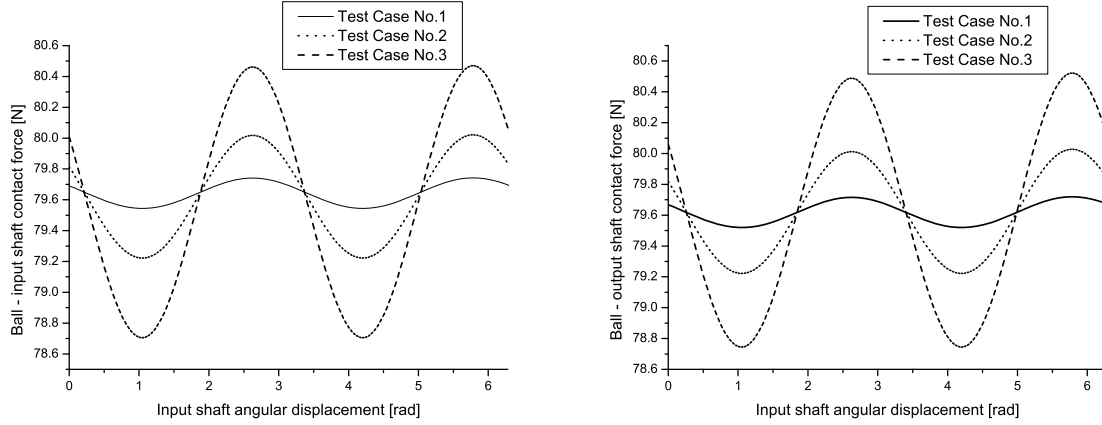


Figure 8: Dynamic analysis of Rzeppa pilot lever joint

The transmission ratios computed from the multibody dynamic simulations are plotted in Figure 5. The plots could be otherwise obtained directly from (3) letting $d = 0$ and substituting (7) into (3).

6 Conclusions

The paper discussed several technical issues associated with the design and dynamic analysis of the pilot-lever Rzeppa joint. It has been proposed a kinematic synthesis procedure for the design of the pilot-lever six bar linkage. The multibody dynamic analysis of the joint allowed to estimate contact forces between the balls and the guide under dynamic conditions. Such analysis is necessary for the gathering of informations for strength and fatigue design of all the joint components.

REFERENCES

- [1] Rzeppa, A.H., Universal Joint, US Patent 2,010,899, 1933
- [2] Rzeppa, A.H., Universal Joint, US Patent 2,046,584, 1934
- [3] Bongiovanni, G., Roccati, G., *Giunti Articolati*, Levrotto e Bella, Torino, Italy, 1984
- [4] Schmelz, F., Seherr-Thoss, H., Aucktor, E., *Universal Joints and Driveshafts*, Springer Verlag, Berlin, 1991
- [5] Wagner, E.R., *Universal Joint and Driveshaft Design Manual*, The Society of Automotive Engineers, 1991

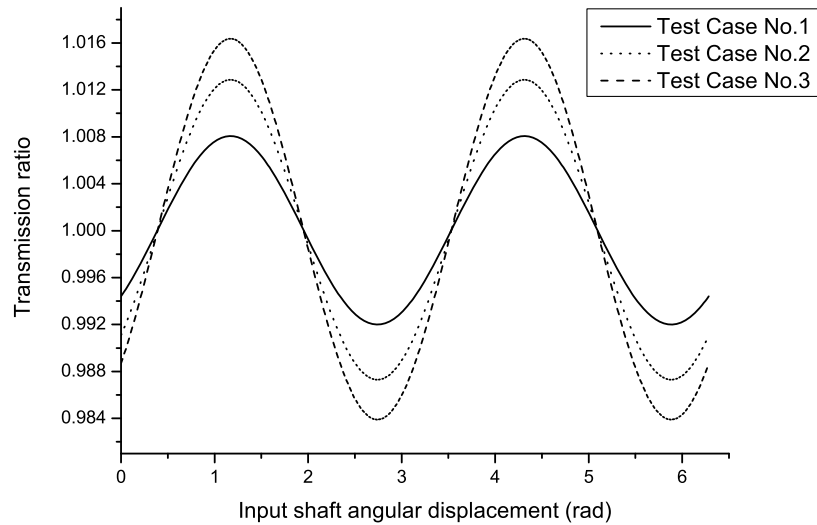


Figure 9: Transmission ratio

- [6] Duditza, F., D. Diaconescu, C. Jaliu, A. Barsan, and M. Neagoe. *Cuplaje Mobile Articulate*. Editura Orientul Latin, Brasov (Romania), 2001.
- [7] Fischer, I.S., Remington, P.M., Errors in Constant-Velocity Shaft Couplings, *ASME Journal of Mechanical Design*, March 1994, vol.116, pp.204-209.
- [8] Fischer, I.S., Lawson, D., Kinematics of the Pilot-Lever Rzeppa Coupling, Proceedings of the 4th National Applied Mechanisms and Robotics Conference, Cincinnati, OH, Dec.1995, Paper AMR-102.
- [9] Cheli, F., Pennestri, E., eds., *Cinematica e Dinamica dei Sistemi Multibody*, Milano, 2006, p.74-79